In-situ Raman spectroscopy analysis of the interface between ceria-containing SOFC anode and stabilized zirconia electrolyte

D.A. Agarkov*, I.N. Burmistrov, F.M. Tsybrov, I.I. Tartakovskii, V.V. Kharton, S.I. Bredikhin

Institute of Solid State Physics RAS, 2 Academician Osipyan Str., Chernogolovka 142432, Moscow Distr., Russia

ARTICLE INFO

ABSTRACT

The combined experimental approach for *in-situ* Raman spectroscopy of the inner "anode|electrolyte" interfaces in solid oxide fuel cells under current load was examined in a case study centered on the behavior of gadolinia-doped ceria (GDC) interlayers between cermet anodes and stabilized zirconia membrane. The Raman spectra of ceria at 850 °C were found sensitive enough with respect to the variations of anodic current and fuel gas mixture composition, which induce oxygen nonstoichiometry changes in GDC. Linear dependence of the Raman peak area on the open-circuit voltage makes it possible to estimate local overpotentials at the GDC interlayer|electrolyte interface under current load. The calculated local overpotentials exhibit a Tafel-like dependence on the current density, and are essentially independent on the hydrogen and water vapor partial pressures within the limits of experimental uncertainties. The relevant rate-determining mechanism may be associated with ion transfer *via* the GDC|zirconia interface, whilst the contributions of exchange-related processes involving gaseous phase are less significant in this interfacial zone.

1. Introduction

Solid oxide fuel cells (SOFCs) are among most promising technologies for the electrical power and heat generation from fossil fuels [1–3]. The SOFC efficiency is strongly dependent on electrode performance [2,3]. One of the most common approaches to increase electrochemical activity of the SOFC anodes is related to the use of ceria-based components such as gadolinia-doped ceria, GDC [4,5]. Ceria is well known as a catalyst for CH_4 [6,7] and CO [8,9] oxidation, also preventing carbon deposition onto the fuel cell anodes [10,11]. The introduction of GDC protective interlayers makes it possible to suppress cation diffusion and chemical reactions between the anode materials and solid-electrolyte membrane. Moreover, doped ceria exhibits fast oxygen ionic transport in combination with a significant electronic conductivity in reducing atmospheres [12,13], which enlarges the electrochemical reaction zone and, thus, enhances anode performance. Due to these properties, ceria is also widely used for oxygen sensors [14,15], hydrogen production [16,17] and other applications.

In previous reports [18,19], a novel combined technique for *in-situ* Raman spectroscopy of SOFC electrodes and simultaneous electrochemical measurements was proposed. This approach was validated studying the kinetics of nickel oxide reduction under the SOFC anode working conditions. The electrode geometry in the model SOFCs, based on optically transparent single-crystal membranes of yttria-stabilized zirconia (YSZ) solid electrolyte, provides an opportunity to directly collect information from the inner interface between the anode and electrolyte [20]. Continuing this research, the present work is centered on the *in-situ* Raman spectroscopy studies of the GDC interlayer|YSZ interfaces under variable current conditions. One particular goal was to evaluate detectability of the current-induced changes in cerium oxidation states and oxygen chemical potential at the SOFC anode|electrolyte interfaces.

2. Experimental

Schematic drawing and photographs of the model cells tested in this work are presented in Fig. 1(a–c). The counter electrode (cathode) has several open circles enabling to pass laser beam through the YSZ single crystal membrane onto the inner interface between YSZ and anode. The solid electrolyte crystals (8YSZ, 8 mol.% Y_2O_3 + 92 mol.% ZrO_2) were produced by the Institute of General Physics RAS (Moscow, Russia); the optically transparent electrolyte disks (thickness of 500 μm, diameter of
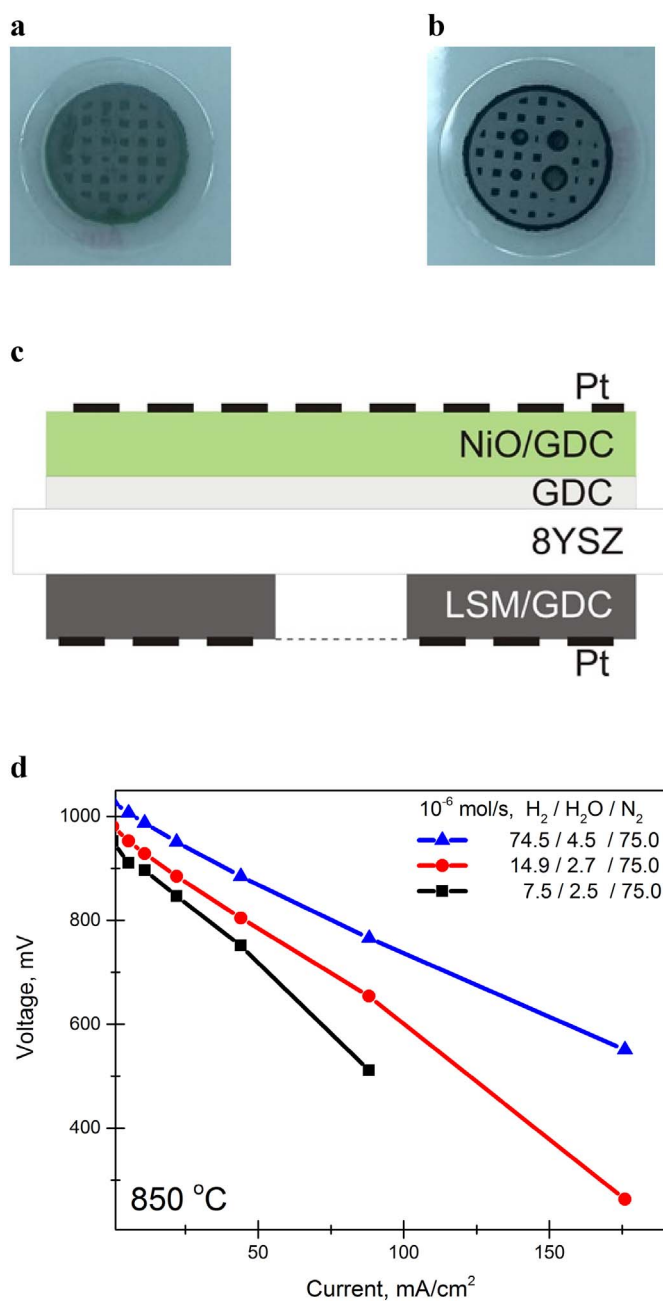
Fig. 1. Photographs of anode (a) and cathode (b) sides of the model SOFC, schematic drawing of the entire cell architecture (c), and examples of I-V curves collected for different fuel mixture compositions at 850 °C (d).

21 mm) were cut with a diamond saw, grinded and polished. The optical transmittance tests [21] showed that the electrolyte membranes transmit more than 70% light energy in the visible light wavelength region.

The equipment and experimental techniques, employed for the electrode deposition and characterization, were described in previous publications [22–24]. The functional Ni-GDC cermet anode layer was applied onto a thin GDC interlayer made of commercial submicron $Gd_{0.1}Ce_{0.9}O_{1.95}$ powder (10GDC, Fuel Cell Materials, USA). During preparation, the powder was annealed in air at 700 °C and then mixed

with Heraeus V006A thinner (mass ratio of 1:1) in a planetary mixer Thinky ARE-250 (Japan). The resultant GDC paste was screen-printed on the single crystal membranes using an Ekra E2 instrument (Asys, Germany) and dried in air at 130 °C. The functional anode layer was prepared from NiO (Sigma Aldrich) and 10GDC, both pre-annealed in air at 700 °C. After mixing of the submicron powders (weight ratio of 1:1) and adding 40 wt% Heraeus V006A, the anode paste was screen-printed onto the GDC interlayer. The anode was sintered at 1300 °C for 2 h; reduction of NiO in flowing H_2-N_2 gas mixture was performed at the initial stage of the Raman measurements. The cathode of $(La_{0.8}Sr_{0.2})_{0.95}MnO_{3-\delta}$ - 10GDC composite (50:50 wt%) was screen-printed onto the opposite side of the single-crystal membrane and annealed at 1100 °C for 2 h. Finally, platinum current-collecting layers made of Heraeus CL11-5100 paste were deposited onto each electrode and sintered in air at 950 °C for 3 h. Typical I-V curves of one model cell, collected at different compositions of the fuel gas mixture supplied onto the anode, are shown in Fig. 1(d).

The experimental setup used in this work was described elsewhere [19]. Briefly, this setup comprises a high-temperature chamber with a single-crystal sapphire sample holder, equipped with Pt wire current collectors, gas communications and several thermocouples. The model fuel cell is pressed and sealed onto open end of the sapphire tube placed in a tubular furnace; a flowing fuel gas mixture is supplied inside this tube using Bronkhorst mass-flow controllers (The Netherlands). In this work, humidified H_2-N_2 mixtures were used as fuel; the SOFC cathode was exposed to atmospheric air. The electrochemical measurements were carried out using a Solartron 1287 potentiostat-galvanostat (UK). The optical part for scattered radiation registration comprises a green laser (532 nm), 2 couples of collecting lenses, crossed optical gap, an optical microscope with CCD-camera, monochromator and a CCD camera (1340 × 100 pixels) with liquid nitrogen cooled sensor; the optical scheme and parameters of the Raman measurements can be found in Ref. [19].

3. Results and discussion

At the first stage of the *in-situ* Raman spectroscopy studies of GDC interlayer|YSZ membrane interface, effects of the fuel gas mixture composition were examined. Fig. 2(a) compares the Raman spectra collected at 850 °C under open-circuit conditions, when the mixtures with H_2/N_2 ratio of 1/10, 1/5 and 1/1 were supplied onto the layered anode. The variations of the hydrogen partial pressure lead, first of all, to systematic changes in the region of $460\,cm^{-1}$ peak; the literature data [25] show that this signal is quite sensitive to the oxygen content variations in ceria and corresponds to symmetric oscillations of oxygen in the fluorite-type crystal lattice. These changes become more visible in the same Raman spectra normalized to the strongest peak of cubic zirconia [26], Fig. 2(b). The inset in Fig. 2(c) illustrates the procedure of the background subtraction used for further refinement. The ground line was approximated by a 3rd order polynomial with the derivative at the $460\,cm^{-1}$ peak edges equal to the initial spectrum derivative. The subtraction results (Fig. 1c) make it possible to extract the correlation between the oxygen chemical potential and peak area. The latter was calculated by integrating the Raman scattering intensity around the target peak, in the Raman shift range of 379–$517\,cm^{-1}$. The relationship between the peak area and open-circuit voltage (OCV) determined by the Nernst equation is linear, Fig. 2(d).

Fig. 3(a) displays the Raman spectra measured as a function of current density across the SOFC anode. These data correspond to an intermediate fuel gas mixture composition ($H_2/H_2O/N_2$ flow ratio of $14.9/2.7/75.0 \cdot 10^{-6}\,mol/s$) and current load range from 0 to
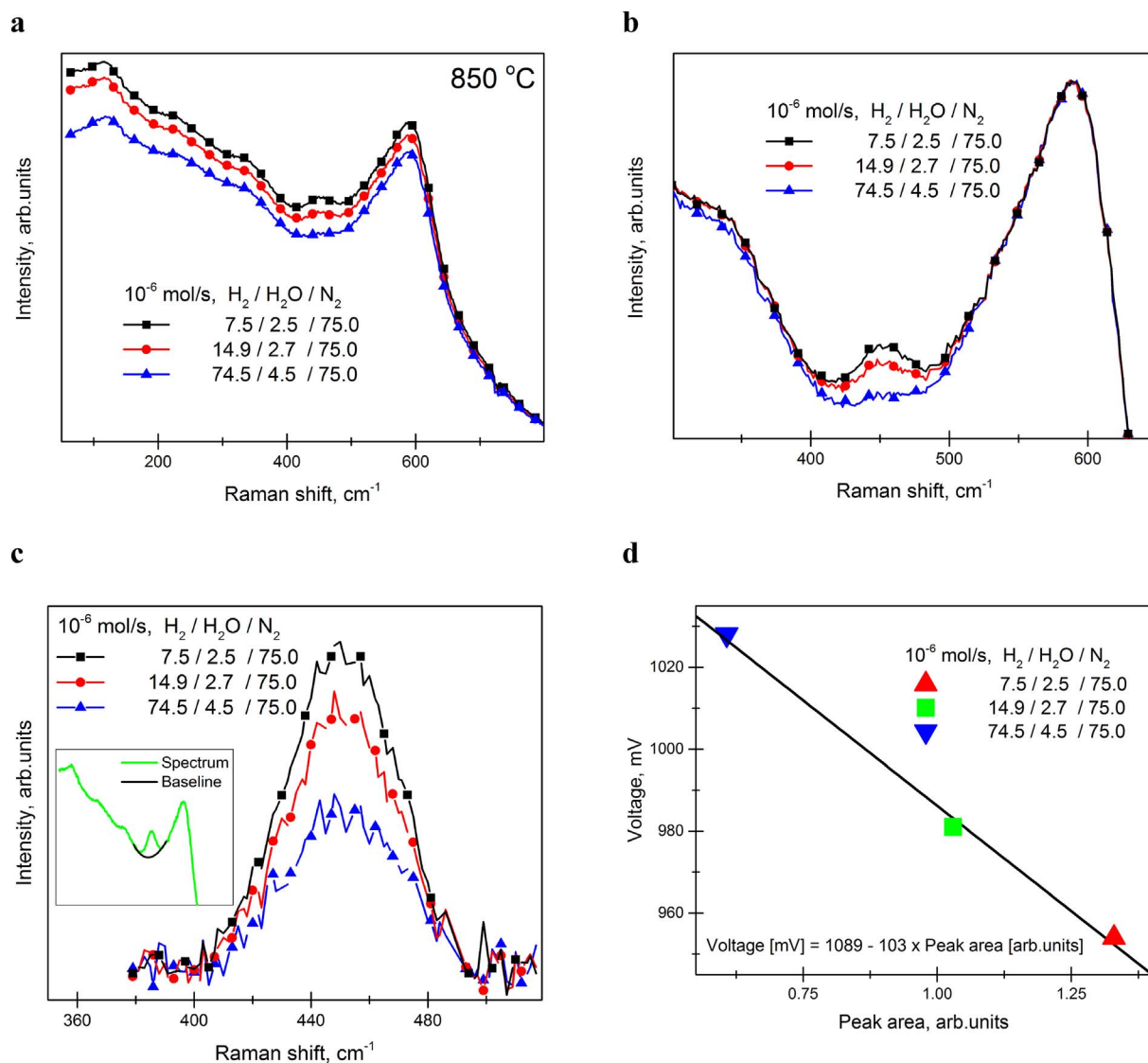
Fig. 2. As-collected Raman spectra *vs.* fuel gas mixture composition under open-circuit conditions at 850 °C (a), the same spectra normalized to the intensity of strongest zirconia peak (b), characteristic $460\,cm^{-1}$ peak after background spectrum subtraction (c), and linear relationship between open-circuit voltage and $460\,cm^{-1}$ peak area (d).

$176\,mA/cm^2$. Again, the $460\,cm^{-1}$ peak intensity is substantially dependent of the current density, whilst other parts of the spectra remain almost unchanged. Notice that similar results were obtained in the entire range of the fuel gas mixture compositions. As for the previous case, all the spectra were normalized to the intensity of strongest zirconia peak (Fig. 3b), followed by subtraction of the background spectrum, Fig. 3(c). The calculated peak area *vs.* current density dependencies in various atmospheres are presented in Fig. 3(d). The Tafel-like shape of these curves can be easily understood if taking into account the linear correlation between the Raman peak intensity and oxygen chemical potential at the anode under open-circuit conditions (Fig. 2d).

Furthermore, the linear relationship shown in Fig. 2(d) enables an estimation of local overpotential at the GDC interlayer|solid electrolyte interface, *i.e.* the current-induced deviation of the local chemical potential of oxygen from its equilibrium value. At a fixed composition of gaseous phase, such a deviation can be derived from the difference between peak areas under a given current density and

under open-circuit conditions using the linear regression model parameters (Fig. 2d). Of course, this interpolation may only be applied in the studied range of the oxygen partial pressures, when oxygen nonstoichiometry of ceria is strongly dependent of the oxygen chemical potential. The extrapolation towards higher $p(O_2)$ and towards pure dry hydrogen require an additional validation.

The estimated overpotentials (Fig. 4a) exhibit a Tafel-like dependence on the current load, as expected. One important feature is that the local overpotential at the GDC|YSZ interface is exclusively determined by the current density and remains independent of the fuel gas mixture composition within the limits of experimental uncertainties. This fact, and an essentially constant slope of the Tafel-like dependence (Fig. 4b), suggest that the rate-limiting mechanism in the interfacial zone is relatively simple and may be associated with anion transfer *via* the interface. The calculated slope of η_{local} *vs.* $\ln(i)$ dependence is equal to $RT/(2\,nF)$ with $n = 2.2 \pm 0.1$. Taking into account the substantial scattering of experimental data points (Fig. 4b), this slope is considered close enough to the theoretical value, 2. The contribution of exchange-
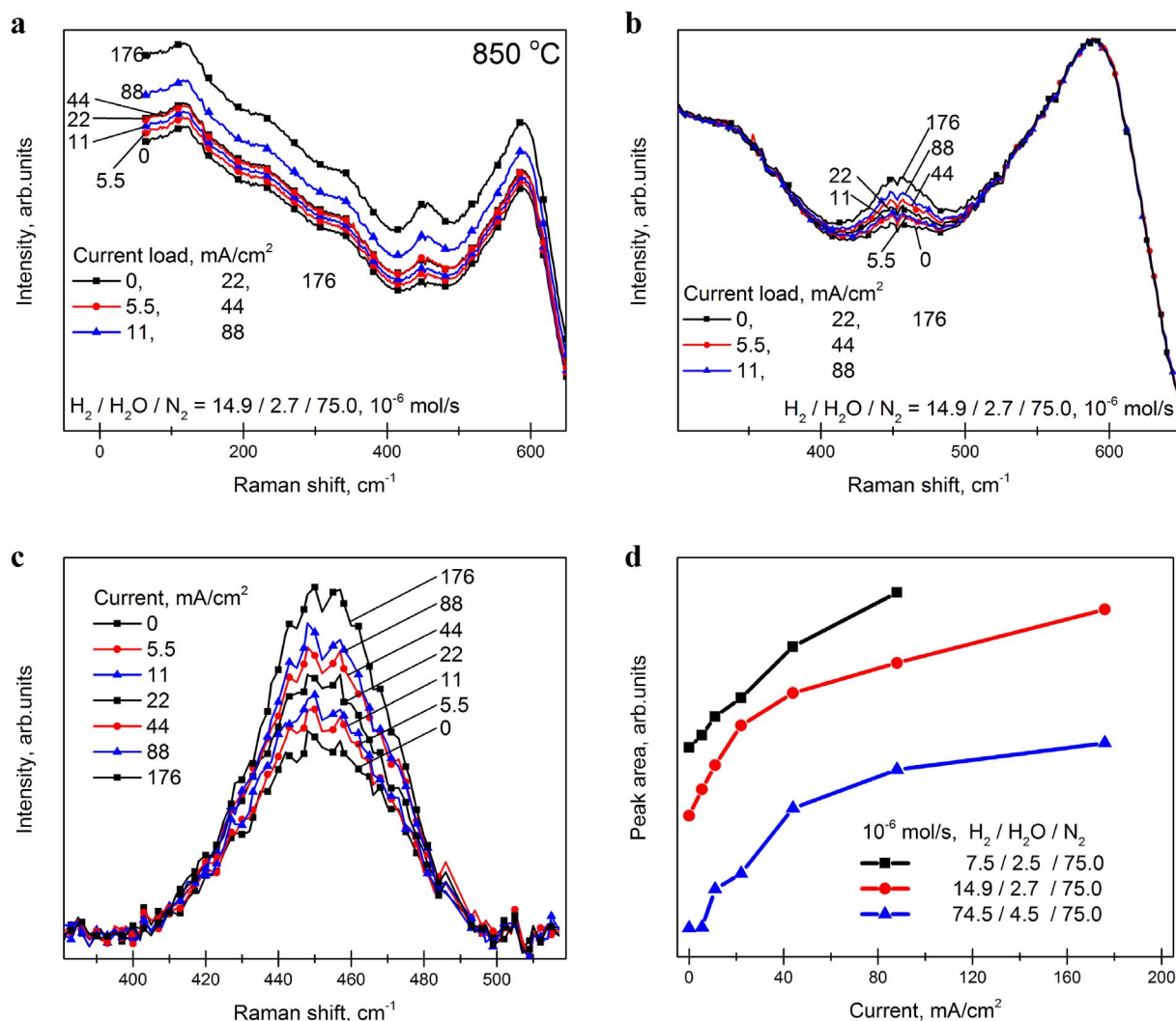
Fig. 3. Variations of the Raman spectra under current load: (a), the spectra collected after equilibration at different current densities; (b), normalization to the intensity of strongest zirconia peak; (c), characteristic peak after background subtraction; (d), dependence of 460 cm^{-1} peak area on the current density at 850 °C.

related processes involving gaseous phase, such as hydrogen oxidation on the GDC surface or in the vicinity of triple-phase boundary, seems less significant. A similar situation is observed for the electronic transport in GDC, which is dependent on the oxygen partial pressure and, hence, H_2:H_2O concentration ratio. At the same time, one should note that the estimated local overpotential probed at the GDC|YSZ interface may only be considered as a part of electrode polarization losses. The total overpotential losses, which can be evaluated from the I-V dependencies of the model cell (Fig. 1d), are up to 5–8 times higher than the local overpotentials and are dependent on the H_2:H_2O ratio. This means that the local current-induced deviations of the oxygen chemical potential from its equilibrium value at the GDC|YSZ interface correspond to the first step of the anodic process. This step, namely ion transfer *via* the interface, is followed by the electrochemical hydrogen oxidation and electron exchange in the anode functional layer.

4. Conclusions

The new combined technique for *in-situ* Raman spectroscopy of the inner SOFC interfaces between the anode and zirconia solid electrolyte membrane under current load was tested for the case studies focused on the protective gadolinia-doped ceria interlayers. The area of 460 cm^{-1} Raman peak of ceria, sensitive to the oxygen nonstoichiometry, exhibits detectable variations with the anodic current and hydrogen partial pressure. The normalized peak area *vs.* OCV dependence makes it possible to analyze local overpotentials at the GDC interlayer|electrolyte interface. Under isothermal conditions, the estimated local overpotentials are exclusively determined by the current density. This dependence can be linearized in the Tafel coordinates in the entire studied range of the fuel gas mixture compositions. The relevant rate-determining mechanisms may be associated with ion transfer *via* the GDC|YSZ interface. The subsequent rate-limiting steps, such as electrochemical hydrogen oxidation in the Ni-GDC layer, are indetectable for the tested anode architecture due to limited laser beam penetration depth. In order to investigate these steps by the *in-situ* Raman spectroscopy, the triple-phase boundary should be directly formed on the YSZ single crystal.
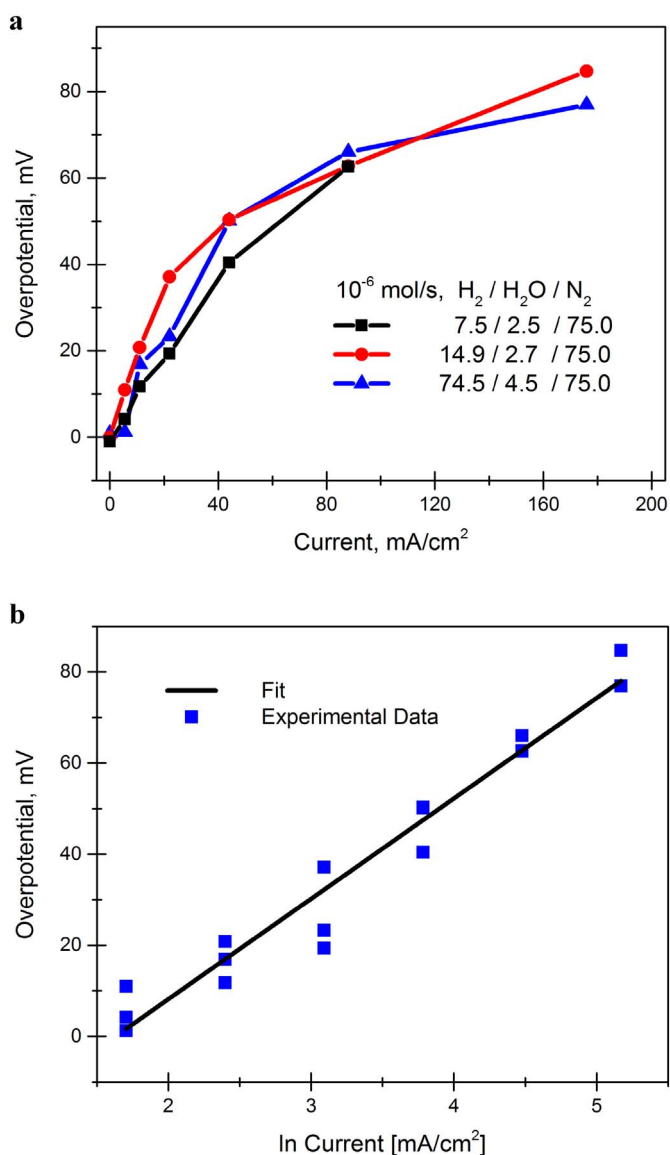
Fig. 4. Estimated local overpotential at the GDC|YSZ interface *vs.* current load (a), and its Tafel-like dependence (b).

References

[1] J.P.P. Huijsmans, F.P.F. van Berkel, G.M. Christie, J. Power Sources 71 (1998) 107.
[2] J. Rossmeisl, W.G. Bessler, Solis state, Ionics 178 (2008) 1694.
[3] T. Takeguchi, R. Kikuchi, T. Yano, K. Eguchi, K. Murata, Catal. Today 84 (2003) 217.
[4] W.C. Chueh, Y. Hao, W. Jung, S.M. Haile, Nat. Mater. 11 (2012) 155.
[5] O.A. Marina, C. Bagger, S. Primdahl, M. Mogensen, Solid State Ionics 123 (1999) 199.
[6] E.P. Murray, T. Tsai, S.A. Barnett, Nature 400 (1999) 649.
[7] J.B. Wang, J.-C. Jang, T.-J. Huang, J. Power Sources 122 (2003) 122.
[8] M. Homel, T.M. Gür, J.H. Koh, A.V. Virkar, J. Power Sources 195 (2010) 6367.
[9] A. Atkinson, S. Barnett, R.J. Gorte, J.T.S. Irvine, A.J. McEvoy, M. Mogensen, S.C. Singhal, J. Vohs, Nat. Mater. 3 (2004) 17.
[10] T. Kim, G. Liu, M. Boaro, S.-I. Lee, J.M. Vohs, R.J. Gorte, O.H. Al-Mahdi, B.O. Dabbousi, J. Power Sources 155 (2006) 231.
[11] N. Laosiripojana, W. Sutthisripok, S. Assabumrungrat, Chem. Eng. J. 112 (2005) 13.
[12] S. Wang, T. Kobayashi, M. Dokiya, T. Hashimoto, J. Electrochem. Soc. 147 (2000) 3606.
[13] J. Faber, C. Geoffroy, A. Roux, A. Sylvestre, P. Abelard, Appl. Phys. A Mater. Sci. Process. 49 (1989) 225.
[14] P. Jasinski, T. Suzuki, H.U. Anderson, Sensors Actuators B Chem. 95 (2003) 73.
[15] N. Izu, W. Shin, I. Matsubara, N. Murayama, J. Electroceram. 13 (2004) 703.
[16] B. Zhang, X. Tang, Y. Li, Y. Xum, W. Shen, Int. J. Hydrog. Energy 32 (2007) 2367.
[17] J. Xu, C.M.Y. Yeung, J. Ni, F. Meunier, N. Acerbi, M. Fowles, S.C. Tsang, Appl. Catal., A 345 (2008) 119.
[18] D.A. Agarkov, I.N. Burmistrov, F.M. Tsybrov, I.I. Tartakovskii, V.V. Kharton, S.I. Bredikhin, Solid State Ionics 302 (2017) 133.
[19] D.A. Agarkov, I.N. Burmistrov, F.M. Tsybrov, I.I. Tartakovskii, V.V. Kharton, S.I. Bredikhin, Russ. J. Electrochem. 52 (2016) 600.
[20] I.N. Burmistrov, D.A. Agarkov, I.I. Tartakovskii, V.V. Kharton, S.I. Bredikhin, ECS Trans. 68 (2015) 1265.
[21] D.A. Agarkov, (PhD Thesis), Institute of Solid State Physics RAS, Russia (2017) 51.
[22] I. Burmistrov, D. Agarkov, S. Bredikhin, Yu. Nepochatov, O. Tiunova, O. Zadorozhnaya, ECS Trans. 57 (2013) 917.
[23] I.N. Burmistrov, D.A. Agarkov, F.M. Tsybrov, S.I. Bredikhin, Russ. J. Electrochem. 52 (2016) 669.
[24] I.N. Burmistrov, D.A. Agarkov, E.V. Korovkin, D.V. Yalovenko, S.I. Bredikhin, Russ. J. Electrochem. 53 (2017) 873.
[25] J.R. McBride, K.C. Hass, B.D. Poindexter, W.H. Weber, J. Appl. Phys. 76 (1994) 2435.
[26] K. Nomura, Y. Mizutani, M. Kawai, Y. Nakamura, O. Yamamoto, Solid State Ionics 132 (2000) 235.